npj | flexible electronics

www.nature.com/npjflexelectron

ARTICLE OPEN

Check for updates

Switchable photothermal conversion efficiency for reprogrammable actuation

Yongcheng He[1], Haojun Liu[1], Jiajia Luo[1], Nuo Li[1], Lihua Li[2], Puxian Xiong[1], Jiulin Gan[1]✉ and Zhongmin Yang[1,2]✉

Reprogrammable soft matter brings flexibility to soft robots so that they can display various motions, which is flourishing in soft robotics. However, the reprogramming of photoresponsive materials used in soft robots is time-consuming using existing methods. In this study, we promote a strategy for rapid reprogramming via switchable photothermal conversion efficiency (PCE). The liquid crystalline elastomers doped with semiconductor bismuth compounds (Bi-LCE) used in this work exhibited large photothermal actuation with over 35% shrinkage in 5 s at high PCE state, which demonstrated little deformation at low PCE state. Furthermore, the material was capable of being reprogrammed up to 10 times, with only 20 min required for one PCE reversible switch. Based on this switchable PCE effect, the same Bi-LCE film displayed various shape changes through different programmable pattern. Additionally, a reprogrammable hollow tube made of PCE reprogrammable materials could tune the diameter, cross-section configuration, and surface morphology, which was crucial for microfluidics field. Reprogrammable materials provide endless possibilities for reusability and sustainability in robotics.

npj Flexible Electronics (2023)7:47 ; https://doi.org/10.1038/s41528-023-00281-0

INTRODUCTION

The controlled actuation of soft matter is an emerging field in robotics owing to its ability to safely interact with fragile and dynamic environments[1]. Significant developments in soft matter have been reported in recent years with high demands for multifunctionality and accuracy in soft robots[2–4]. Soft matter nowadays has now manifested large reversible shape changes with various stimuli programmatically and accurately, paving the path for soft robots to execute complicated actions such as walking[5], jumping[6], and swimming[7]. Light has become a preferred stimulus for soft matter and soft robots for its excellent addressability and spatial-temporal control[8,9]. However, most photoresponsive soft matter currently can only exhibit single-mode deformations once programed during preparation. Multi-mode deformations require more actuation components, which multiplies the difficulty and expenditure of manufacture and control[10,11].

Therefore, many researchers worldwide have focused their attention on reprogrammable soft matter. Reprogrammable soft matter is able to execute different motions through reversibly programmed/erased procedures within the same material, providing remarkable multifunctionality, flexibility, and environmental suitability for soft photoactuators[12,13]. Homogeneous photoresponsive soft materials can be reprogrammed by spatial light control, which shows diverse deformations to cast the light on different parts of the materials with various photomasks during operation[12,14,15]. This complicates the construction and control of the photoactuators and limits the applications. Alternatively, photoresponsive soft materials can be reprogrammable by changing the topology of the networks through the introduction of dynamic covalent chemistry[16]. Prof. Albertus reported a rewritable actuator that can generate various shapes upon light irradiation with different colors of light using a pH-sensitive azomerocyanine dye by acid treatment[17]. Ji et al. developed a thermally reprogrammable liquid crystalline elastomer actuator that relied on siloxane exchange reaction by post-synthesis swelling[18]. However, current photoresponsive reprogrammable soft materials take hours to days to be reprogrammed, which imposes restrictions on practical use.

Heat, a convenient energy, is employed in actuators as it can be easily converted by electricity[19], magnetism[20], and light[21]. Photothermal conversion materials are essential media for photothermal actuation, which require high photothermal conversion efficiency (PCE) and good compatibility of base materials, including organic compounds[22], metal-based nanomaterials[23], carbon-based nanomaterials[24], and semiconductor materials[25]. The actuation materials can be programmed by adjusting the size of the metal-based nanoparticles caused by the localized surface plasmon resonance (LSPR) effect[26]. Once the size of nanoparticles in materials has been determined, it is difficult to change again. On the contrary, semiconductor materials are able to generate hot carriers (i.e., hot electrons and hot holes) under irradiation. These hot carriers first rapidly return to the conduction band and valence band, then equilibrate with the semiconductor lattice and emit phonons to induce photothermal energy[27,28]. Prominent changes in PCE in bismuth materials can be induced by the adjustment of the valence band[29]. If the PCE can be reversibly tuned, it opens an avenue for designing reprogrammable photothermally responsive soft matter. However, few studies have exploited the PCE change in reprogrammable actuation materials.

Here, we propose a reprogrammable photothermally responsive material that takes advantage of the switchable change in photothermal conversion efficiency. The reprogrammable material at the low PCE state remains stationary under low-power illumination, but exhibits slight motion under high-power illumination. Upon switching to the high PCE state, the material

[1]State Key Laboratory Luminescent Materials and Devices, Institute of Optical Communication Materials, Special Glass Fiber and Device Engineering Technology Research and Development Center of Guangdong Province, Guangdong Provincial Key Laboratory of Fiber Laser Materials and Applied Techniques, South China University of Technology, 510641 Guangzhou, China. [2]Future Institute of Technology, School of Information and Optoelectronic Science and Engineering, South China Normal University, 510515 Guangzhou, China. ✉email: msgan@scut.edu.cn; yangzm@scut.edu.cn

displays rapid photothermal conversion, leading to considerable and rapid shape changes under low-power illumination. The fast switchable PCE allows for a high-speed reprogramming procedure, which is conducive to enhancing the multifunctionality and flexibility and tremendously broaden the application scopes of photoresponsive soft materials.

RESULTS

Characterization of reprogrammable photothermally materials

The photothermally responsive materials were able to be reprogrammed by adjusting the PCE as demonstrated in Fig. 1a. The materials could be encoded into various states by different types of masks and then showed different motions under illumination on account of the different PCE of each part. The high PCE part efficiently converted light into a large amount of heat, but the unprogrammable parts were poor at generating heat. The material could also be erased back to its original state for the next program. Our reprogrammable photothermal responsive material also consisted of the actuation base material and the photothermal conversion material. The representative LCE materials prepared by acrylate mesogenic monomers 1,4-*bis*-[4-(6-acryloyloxyhexyloxy)benzoyloxy]-2-methylbenzene, commonly referred to as RM82, was selected as the actuation base material because of its huge thermal uniaxial contraction and stable preparation[30]. Bismuth (III) compounds were chosen for use in the photothermal conversion material because of their fast switchable PCE and high photothermal property[31–33]. We found that the PCE of the bismuth compounds in LCE was capable of changing under UV illumination. As depicted in Fig. 1c, the traditional liquid crystal cell technique was used to prepare the LCE film. Moderate bismuth (III) neodecanoate was added into the precursor as the bismuth source during the preparation. The precursor was composed of the materials shown in Fig. 1b. After heat treatment, oligomer films were formed, which were then uniaxially stretched and UV crosslinked to form bismuth (III)-doped LCE films (Bi-LCE films). As observed in the cross-section of Bi-LCE films (Fig. 1d), nano- to micrometer-sized particles were uniformly distributed in the films without voids or holes in the cross-section. It could be speculated that bismuth compounds were well encircled by LCE networks. Specially, bismuth compounds were possible to be physically incorporated with LCE networks primarily attributed to the significant difference in size between bismuth particles and LCE network molecules. Besides, chemical interactions also existed between bismuth particles and the LCE networks due to the presence of Bi–O coordinate-covalent bonds and Bi–S intermolecular attractions. (Fig. 1e, Supplementary Information and Supplementary Fig. 1).

As the pictures photographed by orthogonal polarized optical microscopy (POM) (Fig. 1f), the Bi-LCE films were in a well uniaxial orientation at room temperature. The Bi-LCE film became softer than the pure LCE film due to the addition of bismuth compound dopants, potentially impeding the crosslinking of the networks. The larger molar ratio of functional groups of thiols between the di-functional flexible spacer (EDDET) and the tetra-functional crosslinking monomer (PETMP) resulted a looser network structure and a softer Bi-LCE film[34]. The softer film presented a larger shortage strain during thermal actuation. However, the film could not fully recover to the original shape when the functional group ratio exceeded 75:25. In order to balance the best mechanical and actuation properties of the film, the functional group ratio of 75:25 of thiols between EDDET and PETMP was chosen to prepare the Bi-LCE film. The Young's modulus of Bi-LCE films was 6.57 MPa (Fig. 1g). According to the differential scanning calorimetry (DSC) diagram (Supplementary Fig. 2), the clearing point of the Bi-LCE film was 88 °C, similar to the pure LCE films. Moreover, the Bi-LCE films showed approximately 45% shrinkage strain at 120 °C (Supplementary Fig. 3), which fed the requirement for actuation.

Photoactuation property of the Bi-LCE films

First, the photoactuation property of the Bi-LCE films in two different states was demonstrated. We designated the Bi-LCE films with high PCE as Bi-LCE-H films and the Bi-LCE films with low PCE as Bi-LCE-L films. In order to maximize the light power utilization, a device was set up as depicted in Fig. 2a. The infrared laser diode (LD) of 808 nm wavelength was used as the excited light source with a spot diameter of nearly 1 cm to drive the Bi-LCE films. Both ends of the Bi-LCE films were glued with tapes to facilitate weight hanging, so that planar motions could be executed rather than the three-dimensional motions caused by the asymmetric orientation produced during preparation, which was a result of manually stretching the oligomer films for uniaxial orientation.

As displayed in Fig. 2b and Supplementary Movie 1, 2, the Bi-LCE-L film contracted at a laser power of 1 W, and the shrinkage strain of the film increased along with increasing the light power. The film reached the maximum shrinkage strain of less than 30% at the light power of 2.5 W. The response time, defined as the time when the film reached 85% of the maximum shrinkage strain, was about 15 s. Then, The Bi-LCE-L film was exposed to both-side UV illumination with a 365-nm wavelength for a duration of 15 min, with the power density of about 30 mW·cm^{-2}. The Bi-LCE-H film was obtained. The Bi-LCE-H film performed shrinkage of over 15% at the light power of 0.5 W and achieved the maximum shrinkage of more than 35% at the light power of 2 W, applying work of approximately 0.05 J by lifting the clamps 200 times its own weight. The smaller photothermal shrinkage compared to the thermal shrinkage might be caused by the light spot of incomplete coverage on the film and the inhomogeneous distribution of the light power. The response time was about 5 s, and the shrinkage strain and the response time promoted little with increasing the light power. All films recovered to their original shape within 5 to 8 s. The Bi-LCE-H films contracted much more sharply than the Bi-LCE-L films, clearly separating two different motion states of the films.

To quantify the photothermal conversion effect, an infrared sensor was set up to detect the surface temperature of the films. The films were irradiated continuously until they reached a steady temperature, followed by cooling to the ambient temperature after the laser was turned off. It could be seen in Fig. 2c that when the samples were irradiated with the infrared laser of 808 nm at the power of 0.757 W, the temperature of the Bi-LCE-H film increased from the ambient temperature of 22.6 °C to 77 °C at the linear rate of about 3 °C s^{-1}. The temperature reached a steady state and then slowly decreased. In contrast, the Bi-LCE-L film was heated warm (32.3 °C) at the same light power. In addition, there was little temperature variation in the pure LCE film, indicating that the networks of LCE contributed little to the thermal conversion. Obviously, there was an enormous difference in the PCE between the Bi-LCE-H film and the Bi-LCE-L film. This was the direct reason for the different photothermal actuation performance of the Bi-LCE films.

Working mechanism of the reprogrammable Bi-LCE film

We attempted to explore the mechanism underlying the switchable PCE in Bi-LCE films. The Bi-LCE film showed an obvious photochromic effect under UV treatment and turned brown owing to the higher absorption in the Bi-LCE-H film (Supplementary Fig. 4), which might be attributed to reversible photochromic effect associated with bismuth compounds, wherein the formation and breakage of short distance bonds cause the color changes[35,36]. Therefore, The X-ray photoelectron spectroscopy (XPS) and Fourier transform infrared (FTIR) spectra for the Bi-LCE films were analyzed to find the changes for the chemical bonds in

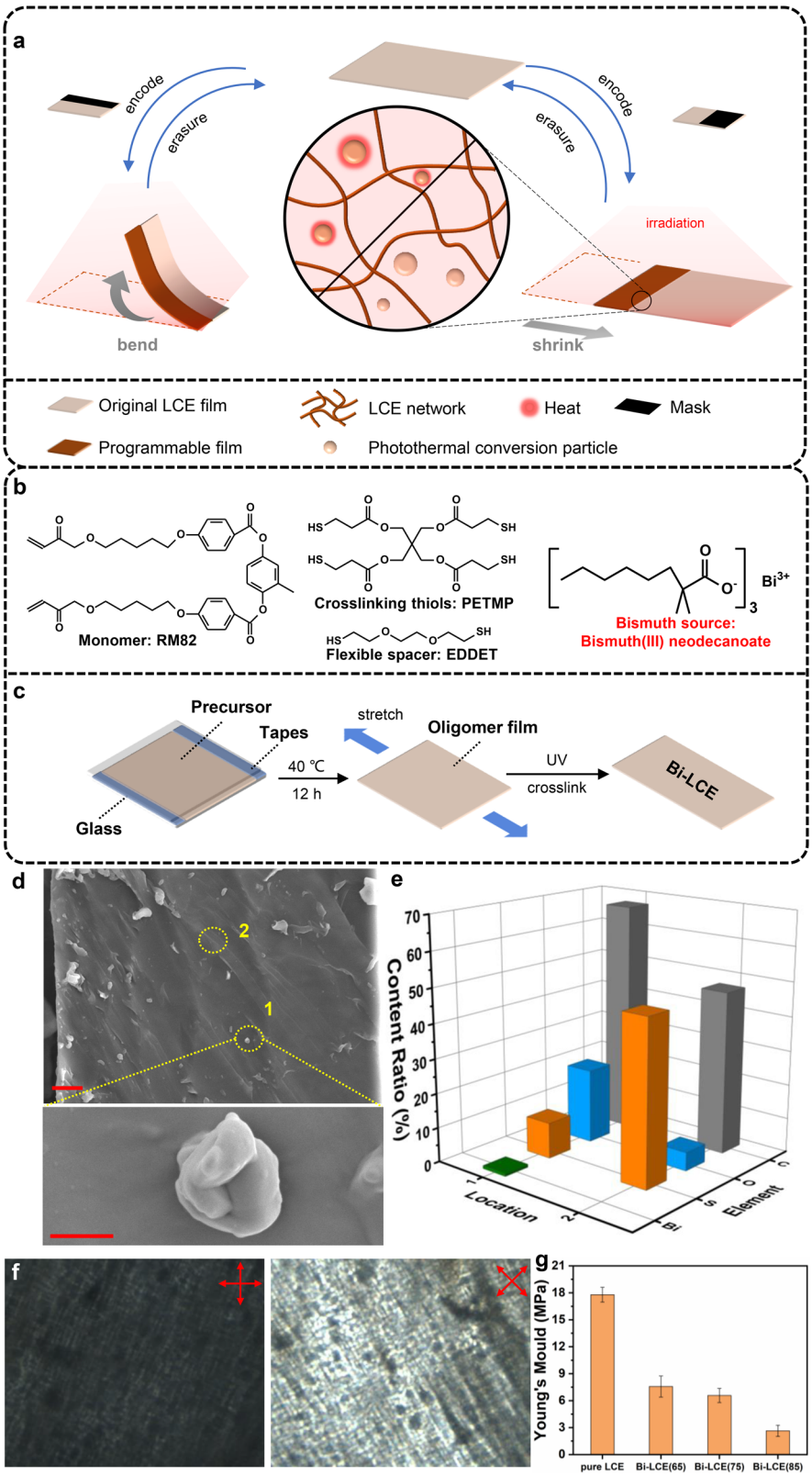

Fig. 1 Reprogrammable photothermally responsive materials. a A sketch of the reprogrammable photothermal materials by adjusting the PCE. **b** The main materials contained in the precursor. **c** The sequence of the Bi-LCE film preparation process. **d** Scanning electron microscope (SEM) images of the cross-section of the Bi-LCE film. Top image showing the microstructure of the Bi-LCE film, with a scale bar of 10 μm. Bottom image zooms in on a bismuth compound particle within the Bi-LCE film, with a scale bar of 1 μm. **e** Content ratio of each element in the cross-section of the Bi-LCE film at different locations, detected by energy disperse spectroscopy (EDS). **f** The images of the Bi-LCE film photographed by polarizing optical microscope (POM) at 5x magnification, left: dark field, right: bright field. **g** Young's mold of the pure LCE film and Bi-LCE film. Tensile tests were conducted three times for each material sample. The bars are the average values of three samples and the error bars represent the standard deviation of each material.

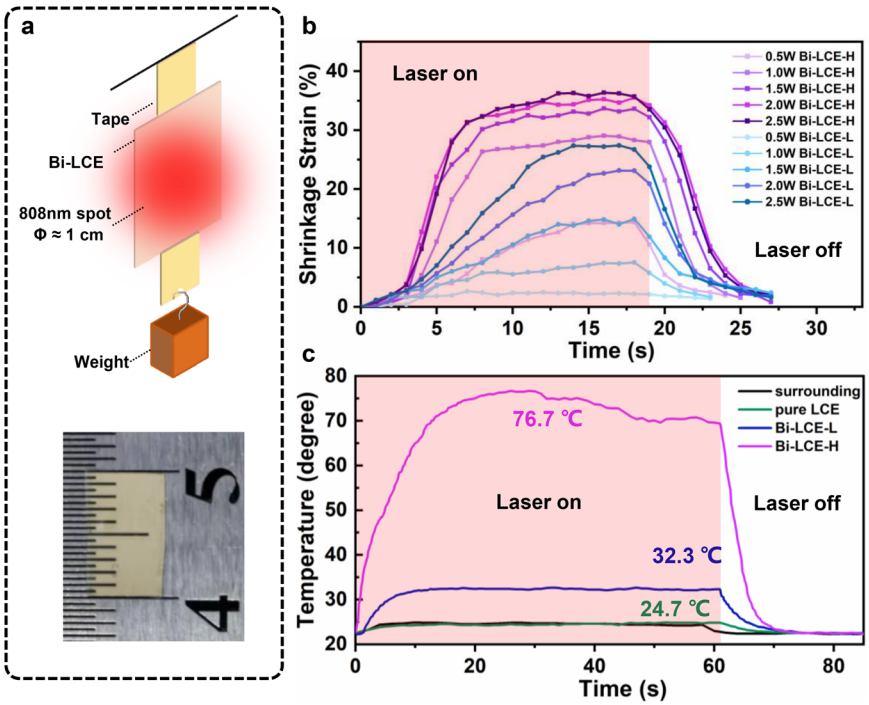

Fig. 2 Photoactuation property of the Bi-LCE films. a Top: Schematic of the devices in the photoactuation performance. Bottom: Images of a Bi-LCE film used in the performance with the size of 10 mm × 5 mm. **b** Shrinkage strain of the Bi-LCE-H and Bi-LCE-L film during photoactuation with different light powers. **c** Temperature variation of the film under infrared illumination.

the films. The XPS spectra of sulfur 2p and bismuth 4f for Bi-LCE-L, Bi-LCE-H, and Bi-LCE-10 films were exhibited in Fig. 3a. The peaks at around 164.5 eV and 159.0 eV before UV treatment were consistent with the binding energy of bismuth 4f5/2 and 4f7/2, similar to the value for Bi_2S_3 and Bi_2O_3[37]. Hence, the valence state of bismuth (III) stayed unchanged before and after UV treatment. Besides, the XPS spectra of S 2p of the Bi-LCE films also demonstrated that there were also changes in sulfur. Three groups of double peaks at around 169.2 eV and 168.0 eV, 167.1 eV and 166 eV, as well as 164.4 eV and 163.3 eV were detected in the Bi-LCE film, which were similar to the value of sulfur 2p3/2 and 2p1/2 for R-SO_2-R bonds, R-S = O-R bonds and C-S bonds, respectively[38–41]. The apparent decline from Bi-LCE-L to Bi-LCE-H films in the binding energy of bismuth from 159.4 eV to 158.9 eV, as well as in the binding energy of sulfur from 163.6 eV to 163.2 eV, indicated that there were more Bi–S bonds in the Bi-LCE-H film[42], which could also be confirmed in FTIR spectra (Fig. 3c and Supplementary Information). Furthermore, the spectra of O 1 s in Fig. 3b revealed two peaks at around 533.5 eV and 532.4 eV, which were assigned to C = O bonds or C–OH bonds and C–O or Bi–O bonds, respectively[43,44]. Significant differences in intensity between the peaks at around 533.5 eV and 532.4 eV with obvious shift could be observed, indicating changes in the oxygen relative bonds. Stronger absorption peaks were observed at 692,764 and 897 cm^{-1} in the FTIR spectra, indicating that the concentration of Bi–O bonds increased in the Bi-LCE-H film. While the peaks at 1161 cm^{-1}, which corresponded to the C–O–C asymmetric stretching[45], became weaker after UV treatment, suggesting a reduced presence of C–O–C bonds in the Bi-LCE-H film. Therefore, it could be speculated that when the Bi-LCE-L film went through the UV treatment to be Bi-LCE-H film, the UV light broke the C-O bonds and created a substantial amount of active oxygen, which led to the formation of other chemical bonds such as Bi–O bonds, C = O bonds and C–OH bonds in the Bi-LCE-H film.

In summary, the mechanism of the switchable PCE in Bi-LCE films could be explained as follows. As shown in Fig. 3f, the Bi-LCE-L film with 3.02 eV bandgap (Fig. 3d) exhibited low photothermal conversion efficiency, because it is challenging to absorb the 808-nm-wavelength infrared light with a photon energy of 1.5 eV. In the programmed process, the UV light with a photon energy of 3.4 eV broke the C–O bonds and created lots of active oxygen in the film. Additionally, it provided bismuth atoms better coordination ability to bond with oxygen or sulfur atoms[35]. As a result, bismuth compounds in Bi-LCE-H films existed more Bi–O bonds in [BiO_6] octahedral units and Bi–S bonds. These additional bonds offered more electrons transition channels so that the film absorbed more photons[36], thus leading to the photochromic effect. While strong resistant forces to bond in amorphous Bi-LCE film (Supplementary Fig. 5) led to abundant defects such as vacancies, which brought defect energy in the Bi-LCE-H film, lowering the bandgap to 1.14 eV (Fig. 3e). Therefore, the narrower bandgap of the Bi-LCE-H film due to defects enabled it to absorb more photon energy to produce hot electrons and holes, facilitating heat generation through electron-phonon scattering and subsequent phonon emission processes, generation vast of heat.

Repetitive and reprogrammable performance of Bi-LCE films

Next, we investigated the performance of the Bi-LCE-H films under repetitive cycling. The infrared light was turned on for 10 s for actuation and turned off for 10 s for recovery, with a light power of 2 W for each cycle. As shown in Fig. 4a and Supplementary Movie 3, the photoresponsive shrinkage actuation was repeated twelve times. It could be observed that the shrinkage strain at the twelfth time declined to about 15% from the initial maximum strain of near 50% in the repetitive cycling photoactuation performance of the Bi-LCE-H films. This reduction in strain could be attributed to the reversible photochromic effect, where the film could revert to its original color under high temperature (~80 °C)[35]. When the temperature increased, intense vibration of the atoms within Bi-LCE films broke the fragile chemical bonds generated by UV illumination. Consequently, the electron transition channels and the defect energy decreased, leading to an enlargement of the

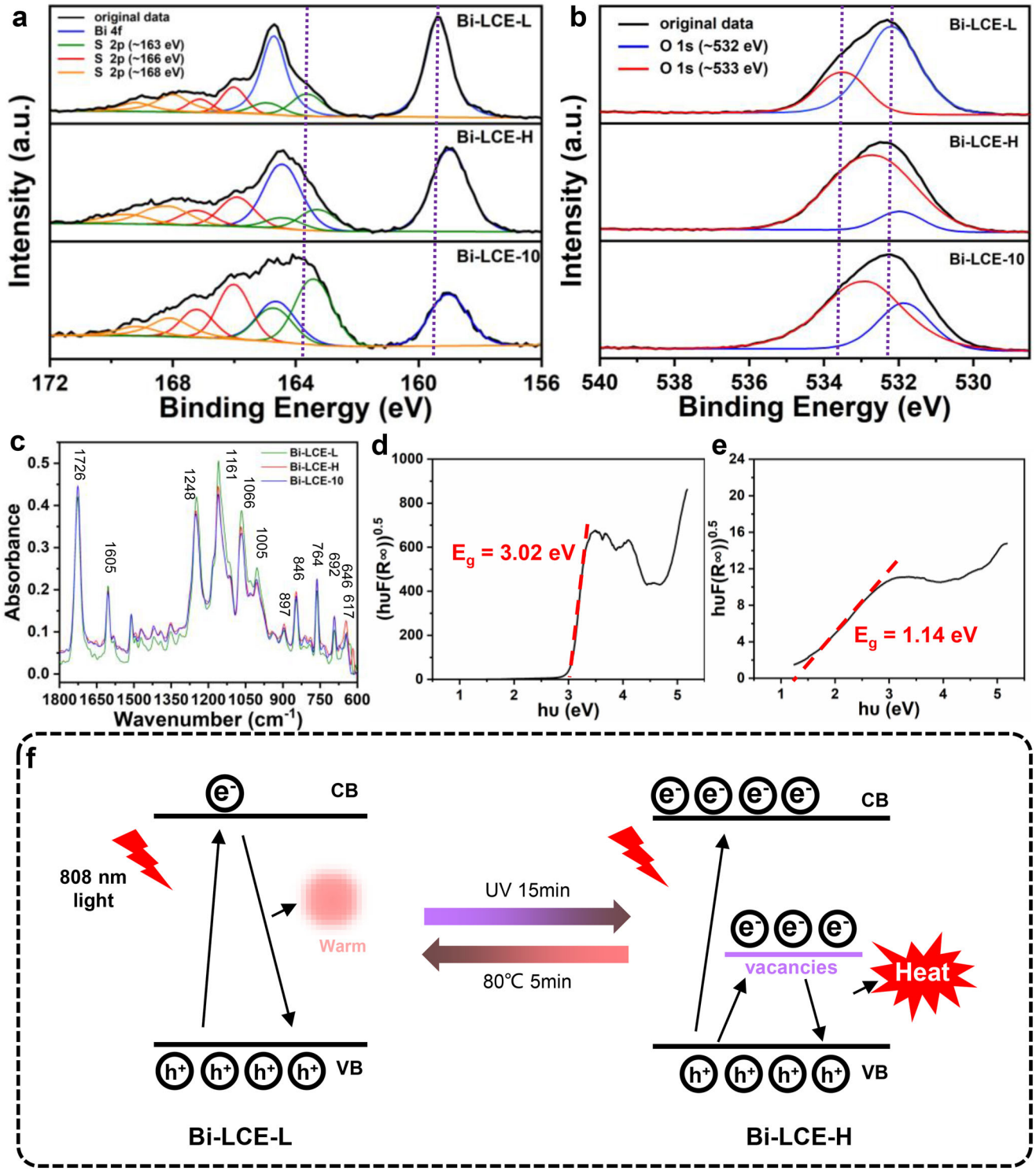

Fig. 3 The mechanism underlying the switchable PCE in Bi-LCE films. The XPS spectra of the Bi-LCE film before UV treatment, after UV treatment and reprogrammed for 10 times of (**a**) Bi 4 f and S 2p. **b** O 1 s. were shown. **c** FTIR spectra of the Bi-LCE film before UV treatment, after UV treatment and reprogrammed for 10 times. The plot of $[F(R\infty)h\nu]^{0.5}$ versus energy (eV) of the Bi-LCE films were shown. **d** Bi-LCE-L. **e** Bi-LCE-H. **f** A proposed mechanism sketches for the switchable photothermal conversion effeciency in Bi-LCE film.

bandgap of the Bi-LCE films. The surface temperature of the film reached over 110 °C when exposed to the infrared light source with the light power of 2 W (Supplementary Fig. 6). Therefore, the heat generated by the infrared light not only actuated the film but also caused it to partly recover to the Bi-LCE-L film, thus weakening the photoactuation property of the film. From the overall effect, the Bi-LCE films demonstrated a sufficient level of repeatability, achieving over 15% shrinkage strain, which was suitable for most applications.

Then, we evaluated the reprogrammable performance of the Bi-LCE films. The Bi-LCE-L film was taken as the original state, which was programmed to become the Bi-LCE-H film using both-side UV

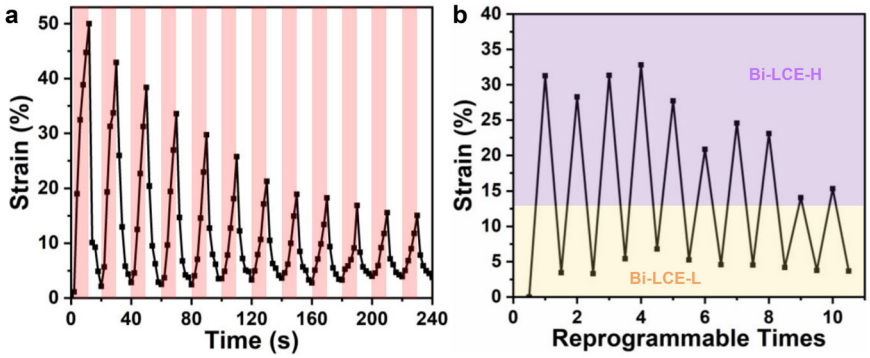

Fig. 4 The repetitive and reprogrammable photoactuation performance of the Bi-LCE films. a The photoactuation performance of the Bi-LCE-H film under repetitive cycling. **b** The reprogrammable performance of the Bi-LCE films.

illumination with a 365-nm wavelength for 15 min. The programmed Bi-LCE-H film could be erased and recovered to the Bi-LCE-L film by heating it in 0.1 wt% EDDET/ethanol solution at 80 °C for 5 min. The entire reprogrammable procedure, including programming and erasing, took only 20 min to complete. The photoactuation performance of the Bi-LCE film was tested after the programming and erasing treatment. Figure 4b and Supplementary Movie 4 exhibited that the Bi-LCE film could be reprogrammed for 10 times. The Bi-LCE-H film, which was programmed for the first time, shrank by about 30% strain. However, the shrinkage strain declined along with the increasing number of programmable times, which descended to over 15% after the tenth programmable procedure. The decline in photoactuation properties after several programmable procedure might be attributed to the stabilization of chemical bonds due to repetitive connection and fracture based on the principle of minimum energy[46]. As the FTIR spectra of Bi-LCE-10 shown in Fig. R2, more Bi–O bonds in [BiO_3] pyramidal structural units and less Bi–O bond in [BiO_6] octahedral units existed in Bi-LCE-10 film, according to the absorbance intensity of the assigned 692 and 764 cm^{-1} peaks. While the lower absorbance intensity of the peaks at 897 cm^{-1} suggested less Bi–O bonds in [BiO_6] octahedral units in Bi-LCE-10 film. Additionally, the active oxygens produced by UV light might replace the S atoms. There were also less Bi–S bonds, C–S bonds, S = O bonds and SO_4 according to the lower absorbance of the peaks at 619 cm^{-1}, 764 cm^{-1} and 846 cm^{-1}, 1248 cm^{-1},1005 cm^{-1} and 1066 cm^{-1}, respectively. These changes in chemical bonds might lead to variations on the bandgap, weakening the photoactuation property after several programmable procedure. The Bi-LCE-L film maintained less than 5% shrinkage strain after ten times of erasure processes, which was similar to the original state. Although there was a slight decline in the photoactuation property after reprogramming processes, the film could reach the same performance by prolonging the exposure time or increasing the irradiation power.

Reprogrammable control applications of Bi-LCE films

The patterning method could be used to create complex deformation patterns with responsive light illumination. Therefore, the same Bi-LCE film could be reprogrammed to present diverse deformations under irradiation. The 11 mm × 6 mm Bi-LCE film was locally covered by three different photomasks to prevent the UV light from encoding the film. As shown in Fig. 5c, e, g, i and Supplementary Movies 5–8, the encoded part of the film turned brown while the covered part remained light. The film was first encoded from the original state (Fig. 5a, b) with a 1-mm strip (Fig. 5c), followed by a 5 mm × 6 mm area (Fig. 5e). Then, two squares with 2 mm sides were programmed in the center of the film (Fig. 5g) and finally three squares were encoded (Fig. 5i). A bandpass filter in the wavelength range of 510 ± 40 nm was used during photography to filter out the red light and to clarify the appearance of the film. Only the brown regions contracted along with the orientation under right above infrared illumination at the light power of 2.5 W. The encoded film under uniform infrared illumination showed different three-dimensional deformations in about 10 s, involving bending, contracting and wrinkling in sequence, as shown in Fig. 5d, f, h and Supplementary Movies 5–7. The film immediately regained its flatness after the light was turned off. The film was erased after the demonstration. Besides, the light power also influenced the shrinkage strain of the film, which also affected the final shape of the film. As demonstrated by Fig. 5j–l and Supplementary Movie 8, the film turned plicated under 1.5W-power infrared illumination whereas it transformed into saddle shape at the light power of 2.5 W. But when the light power was further increased as illustrated in Fig. 5l and Supplementary Movie 8, the final actuation motion varied little because the coded parts reached their maximum shrinkage strain, corresponding to the former performance.

The reprogrammable process is not limited to the plane film. It can also be extended to other structures. For example, a hollow tube (Fig. 6a, b) made of the Bi-LCE film could be patterned with simple UV treatment. The tube had a diameter of 6 mm and a length of 8 mm, and its orientation was vertical to the long side. The infrared illumination was also directly above the tube. Under irradiation, the top surface closer to the light source contracted more than the bottom surface, and the side part of the tube was transformed into a 5-mm diameter oval (Fig. 6c, d and Supplementary Movie 9) at the light power of 2.0 W. Then, the tube was reprogrammed to the configuration shown in Fig. 6e, and the cross-section of the tube was deformed into a flower shape (Fig. 6f and Supplementary Movie 10) at the light power of 3.0 W. While it could not be observed sunk on the left side of the tube, possibly because the encoded part was deflected form the light source and absorbed less light power, resulting in a less pronounced shape change. Next, the tube was encoded again to the configuration shown in Fig. 6g, and it presented the rough surface of the tube (Fig. 6h and Supplementary Movie 11) at a light power of 2.5 W. Therefore, the single tube was able to be reprogrammed to achieve different complicated shapes at once under infrared irradiation with appropriate light power, including the diameter adjustment, cross-sectional configuration, and surface morphology. The encoding and the erasing methods were the same as for the film mentioned above. It was difficult for other molding approaches to realize the complex deformation change. It would be easy to control the speed, quantity and state of the fluid by transforming the shapes of the tube in appropriate programs to the tube, which was highly desirable in microfluidics field.

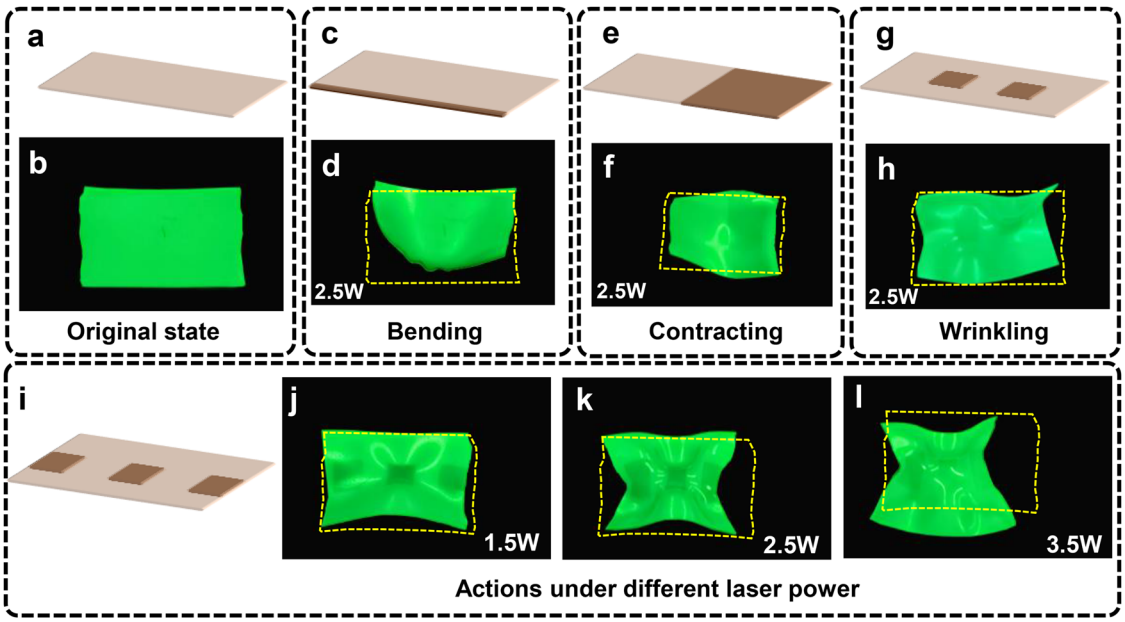

Fig. 5 The Bi-LCE film reprogrammed using the patterning method showed different shapes. The sketch (**a**) and image (**b**) of the original state of Bi-LCE film was showed as above. It showed various motions such as bending (**d**), contracting (**f**) and wrinkling (**h**) along with different programming procedure like the sketches of (**c**), (**e**), and (**g**), respectively. The film with the programming procedure (**i**) displayed different shapes under different light power of 1.5 W (**j**), 2.5 W (**k**), and 3.5 W (**l**). The darker parts of the film were programmed by UV illumination while the lighter parts were covered by photomasks to prevent UV light in the photos. The dotted lines represented the initial position of the film. The background of the deformation pictures was modified to black with Photoshop software.

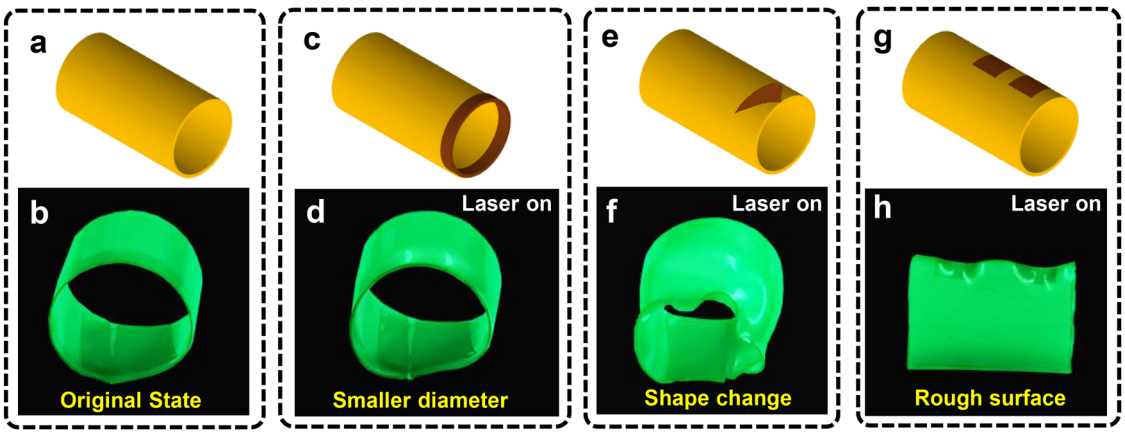

Fig. 6 The same Bi-LCE reprogrammable tube displayed different shapes. The sketch (**a**) and image (**b**) of the original state of Bi-LCE tube are shown as above. The tube was also first encoded into (**c**) a 1-mm strip and then (**e**) an isosceles right triangle with 5 mm right-angle sides on the edges of the tube and finally (**g**) two squares with 2-mm sides on the surface of the tube. The corresponding shape changes of the tube under the appropriate infrared light illumination were shown in (**d**), (**f**), and (**h**), respectively. The background of the deformation pictures was modified to black with Photoshop software.

DISCUSSION

We have developed a reprogrammable photothermally responsive liquid crystalline elastomers adopting a strategy that exploits the switchable photothermal conversion efficiency. The material enables quick and easy encoding or erasure, without the need for complicated processes like physical cutting or chemical patterns. It exhibits rapid photoactuation and significant deformation after programming. Accordingly, the material also displays reprogrammability in three-dimensional form. This reprogrammable soft matter represents a recyclable and sustainable development. It is an exciting strategy for reprogrammable soft matter to have applications in multiple fields such as medicine, microfluidics, robotics and space exploration, which provides infinite possibilities for the manufacture of transformation devices of pre-designed geometric shapes.

METHODS

Materials

In our experiment, the following materials were applied. The monomers were prepared using 1,4-Bis-[4-(6-acryloyloxyhexyloxy) benzoyloxy]-2-methylbenzene (RM82, 125248-71-7) from Shijiazhuang Sdyano Fine Chemical. Bismuth neodecanoate (251-964-6) from Sigma Aldrich was used as the bismuth source. Spacer 2,2′-[1,2-ethanediylbis(oxy)]diethanethiol (EDDET, 14970-87-7) and photoinitiator (Irgaucure 2959, 106797-53-9) was purchased from

TCI, Shanghai. Crosslinker pentaerythritol tetrakis (3-mercaptopropionate) (PETMP, 7575-23-7) and catalyst dipropyl amine (DPA, 142-84-7) were obtained from Aladdin, Shanghai. Dichloromethane (75-09-2) was purchased from Shanghai Macklin Biochemical Co., Ltd.

Preparation of the pure LCE films and the Bi-LCE films

The synthesis of LCE films was in the traditional two-stage method with liquid crystal cell as described in detail by Yakacki et al.[47,48]. Specifically, 0.0145 g of bismuth (III) neodecanoate was mixed with the LCE precursor containing 0.3000 g RM82, 58 µl EDDET, 0.0580 g PETMP, 0.0042 g irgacure 2959, 2 µl DPA and moderate dichloromethane. Particularly, extra thiols were introduced to promote the crosslinking of the LCE networks because bismuth (III) ions could inhibit polymerization of the LCE precursor. The precursor was then dropped onto a clean glass surface with a thin layer of polyvinyl alcohol (PVA) and 100 µm thick packaging tapes affixed to the edges. Next, another clean glass with a PVA layer was carefully placed on top of the frist to get a cell, which was then heated to 40 °C for 12 h. The resulting oligomer LCE film was removed from the cell and uniaxially stretched with the UV illumination for 30 min to fully polymerize the LCE networks. Finally, a Bi-LCE film was obtained. The pure LCE film could be gotten in the same way as long as bismuth (III) neodecanoate was omitted. The films were cut into the desired size for further experiments.

Photoactuation demonstrations

The Bi-LCE films in the photoactuation demonstrations were prepared with a size of 10 mm × 5 mm and a thickness of around 100 µm, weighing 0.0060 g. The infrared laser diode (LD) at the wavelength of 808 nm was used as the excited light source. The infrared light was coupled into a commercial multimode fiber through optical lens, and the Bi-LCE films were illuminated by the infrared light through a collimator equipped at the end of the fiber, which produced a spot diameter of nearly 10 mm. The photoactuation demonstrations were recorded by a smartphone camera, and keyframes were extracted from the videos to obtain photos. Then the pixel coordinates of the top-right end (x_3, y_3) and bottom-right end (x_4, y_4) of the film were taken, and the corresponding pixel coordinates of the original state were (x_1, y_1) and (x_2, y_2). The shrinkage strain ε in the current time was calculated by the following formula (1):

$$\epsilon = \frac{\sqrt{(x_3 - x_4)^2 + (y_3 - y_4)^2}}{\sqrt{(x_1 - x_2)^2 + (y_1 - y_2)^2}} \quad (1)$$

DATA AVAILABILITY

All data needed to evaluate the conclusions in the paper are present in the paper and/ or the Supplementary Materials. Additional data related to this paper are available from the corresponding author upon reasonable request.

Received: 27 May 2023; Accepted: 5 October 2023;
Published online: 20 October 2023

REFERENCES

1. Wang, X. Q. & Ho, G. W. Design of untethered soft material micromachine for life-like locomotion. *Mater. Today* **53**, 197–216 (2022).
2. Hartmann, F., Baumgartner, M. & Kaltenbrunner, M. Becoming sustainable, the new frontier in soft robotics. *Adv. Mater.* **33**, 2004413 (2021).
3. Li, M., Pal, A., Aghakhani, A. & Sitti, M. Soft actuators for real-world applications. *Nat. Rev. Mater.* **7**, 235–249 (2022).
4. Kriegman, S., Blackiston, D., Levin, M. & Bongard, J. A scalable pipeline for designing reconfigurable organisms. *Proc. Natl Acad. Sci.* **117**, 1853–1859 (2020).
5. Cunha, M. P. et al. A soft transporter robot fueled by light. *Adv. Sci.* **7**, 1902842 (2020).
6. Jeon, J. et al. Continuous and programmable photomechanical jumping of polymer monoliths. *Mater. Today* **49**, 97–106 (2021).
7. Li, G. et al. Self-powered soft robot in the Mariana Trench. *Nature* **591**, 66–71 (2021).
8. Wu, X. et al. Light-driven microdrones. *Nat. Nanotechnol.* **17**, 477–484 (2022).
9. Nie, Z. Z. et al. Light-driven continuous rotating Möbius strip actuators. *Nat. Commun.* **12**, 1–10 (2021).
10. Wang, Y. et al. 3D-printed photoresponsive liquid crystal elastomer composites for free-form actuation. *Adv. Funct. Mater.* **33**, 2210614 (2022).
11. Keneth, E. S., Kamyshny, A., Totaro, M., Beccai, L. & Magdassi, S. 3D printing materials for soft robotics. *Adv. Mater.* **33**, 2003387 (2021).
12. Lahikainen, M., Zeng, H. & Priimagi, A. Reconfigurable photoactuator through synergistic use of photochemical and photothermal effects. *Nat. Commun.* **9**, 4148 (2018).
13. Zhao, C. et al. Thermal/near-infrared light dual-responsive reconfigurable and recyclable polythiourethane/CNT composite with simultaneously enhanced strength and toughness. *Macromol. Rapid Commun.* **44**, e2200806 (2022).
14. Hauser, A. W., Evans, A. A., Na, J. H. & Hayward, R. C. Photothermally reprogrammable buckling of nanocomposite gel sheets. *Angew. Chem.* **127**, 5524–5527 (2015).
15. Zhuang, X. et al. Active terahertz beam steering based on mechanical deformation of liquid crystal elastomer metasurface. *Light.: Sci. Appl.* **12**, 14 (2023).
16. Lu, X. et al. 4D-printing of photoswitchable actuators. *Angew. Chem. Int. Ed.* **60**, 5536–5543 (2021).
17. Gelebart, A. H., Mulder, D. J., Vantomme, G., Schenning, A. P. H. J. & Broer, D. J. A rewritable, reprogrammable, dual light-responsive polymer actuator. *Angew. Chem.* **129**, 13621–13624 (2017).
18. Wu, Y. et al. Liquid-crystalline soft actuators with switchable thermal reprogrammability. *Angew. Chem.* **132**, 4808–4814 (2020).
19. Tan, M. W. M., Bark, H., Thangavel, G., Gong, X. & Lee, P. S. Photothermal modulated dielectric elastomer actuator for resilient soft robots. *Nat. Commun.* **13**, 6769 (2022).
20. Zou, B. et al. Magneto-thermomechanically reprogrammable mechanical metamaterials. *Adv. Mater.* **35**, 2207349 (2023).
21. Wang, Y. et al. Light-activated shape morphing and light-tracking materials using biopolymer-based programmable photonic nanostructures. *Nat. Commun.* **12**, 1651 (2021).
22. Liu, L., Liu, M. H., Deng, L. L., Lin, B. P. & Yang, H. Near-infrared chromophore functionalized soft actuator with ultrafast photoresponsive speed and superior mechanical property. *J. Am. Chem. Soc.* **139**, 11333–11336 (2017).
23. He, Y. et al. Optical fiber waveguiding soft photoactuators exhibiting giant reversible shape change. *Adv. Opt. Mater.* **9**, 2101132 (2021).
24. Xiao, J. et al. Optical fibre taper-enabled waveguide photoactuators. *Nat. Commun.* **13**, 363 (2022).
25. Wang, L. et al. Multi-functional bismuth-doped bioglasses: combining bioactivity and photothermal response for bone tumor treatment and tissue repair. *Light.: Sci. Appl.* **7**, 1 (2018).
26. Lan, T., Hu, Y., Wu, G. & Chen, W. Wavelength-selective and rebound-able bimorph photoactuator driven by a dynamic mass transport process. *J. Mater. Chem. C.* **3**, 1888–1892 (2015).
27. Nozik, A. J. Spectroscopy and hot electron relaxation dynamics in semiconductor quantum wells and quantum dots. *Annu. Rev. Phys. Chem.* **52**, 193–231 (2001).
28. Li, B. et al. Improving the photothermal therapy efficacy and preventing the surface oxidation of bismuth nanoparticles through the formation of a bismuth@bismuth selenide heterostructure. *J. Mater. Chem. B* **8**, 8803–8808 (2020).
29. Zheng, N. et al. Responsive degradable theranostic agents enable controlled selenium delivery to enhance photothermal radiotherapy and reduce side effects. *Adv. Healthc. Mater.* **10**, 2002024 (2021).
30. Wang, Y. et al. Repeatable and reprogrammable shape morphing from photoresponsive gold nanorod/liquid crystal elastomers. *Adv. Mater.* **32**, 2004270 (2020).
31. Perez-Mato, J. M. et al. Multiple instabilities in $Bi_4Ti_3O_{12}$: A ferroelectric beyond the soft-mode paradigm. *Phys. Rev. B* **77**, 184104 (2008).
32. Xu, W. et al. Interfacial Bi–S bonds modulate band alignment for efficient solar water oxidation. *Nanoscale* **14**, 14520–14528 (2022).
33. Ma, G. et al. A novel theranostic agent based on porous bismuth nanosphere for CT imaging-guided combined chemo-photothermal therapy and radiotherapy. *J. Mater. Chem. B* **6**, 6788–6795 (2018).
34. Saed, M. O. et al. Thiol-acrylate main-chain liquid-crystalline elastomers with tunable thermomechanical properties and actuation strain. *J. Polym. Sci. B: Polym. Phys.* **55**, 157–168 (2017).
35. Wang, Y. L. et al. Synthesis, crystal structure and photochromic property of a phenethyl viologen bismuth (III) chloride. *J. Coord. Chem.* **72**, 573–583 (2019).

36. Alansi, A. M., Qahtan, T. F., Al Abass, N., Al-Qunaibit, M. & Saleh, T. A. In-situ sunlight-driven tuning of photo-induced electron-hole generation and separation rates in bismuth oxychlorobromide for highly efficient water decontamination under visible light irradiation. *J. Colloid Interf. Sci.* **614**, 58–65 (2022).
37. Morgan, W. E., Stec, W. J. & Van Wazer, J. R. Inner-orbital binding-energy shifts of antimony and bismuth compounds. *Inorg. Chem.* **12**, 953–955 (1973).
38. Yu, X. R., Liu, F., Wang, Z. Y. & Chen, Y. Auger parameters for sulfur-containing compounds using a mixed aluminum-silver excitation source. *J. Electron Spectrosc.* **50**, 159–166 (1990).
39. Su, C. C. & Faller, J. W. Application of electron spectroscopy for chemical analysis to the study of ambidentate binding in sulfoxide complexes. *Inorg. Chem.* **13**, 1734–1736 (1974).
40. Birchall, T., Connor, J. A. & Hillier, L. H. High-energy photoelectron spectroscopy of some antimony compounds. *J. Chem. Soc. Dalton Trans.* **20**, 2003–2006 (1975).
41. Wiegand, B. C., Uvdal, P. & Friend, C. M. Probing the kinetics for thiol desulfurization: the reactions of 2-methyl-2-propanethiol on molybdenum (110). *J. Phys. Chem.* **96**, 4527–4533 (1992).
42. Naik, R., Sahoo, P. P., Sripan, C. & Ganesan, R. Laser induced Bi diffusion in $As_{40}S_{60}$ thin films and the optical properties change probed by FTIR and XPS. *Opt. Mater.* **62**, 211–218 (2016).
43. Li, Q., Song, W., Sun, M., Li, J. & Yu, Z. Response of Bacillus vallismortis sp. EPS to exogenous sulfur stress/induction and its adsorption performance on Cu (II). *Chemosphere* **251**, 126343 (2020).
44. Liao, Y. et al. Bismuth sulfide strongly coupled to functionalized MWNTs hybrids with improved thermoelectric properties. *Adv. Electron. Mater.* **7**, 2100468 (2021).
45. Gwon, J. G., Lee, S. Y., Doh, G. H. & Kim, J. H. Characterization of chemically modified wood fibers using FTIR spectroscopy for biocomposites. *J. Appl. Polym. Sci.* **116**, 3212–3219 (2010).
46. Gutiérrez-Oliva, S., Jaque, P. & Toro-Labbé, A. Using Sanderson's principle to estimate global electronic properties and bond energies of hydrogen-bonded complexes. *J. Phys. Chem. A* **104**, 8955–8964 (2000).
47. Li, Y., Liu, Y. & Luo, D. Polarization dependent light-driven liquid crystal elastomer actuators based on photothermal effect. *Adv. Opt. Mater.* **9**, 2001861 (2021).
48. Yakacki, C. M. et al. Tailorable and programmable liquid-crystalline elastomers using a two-stage thiol–acrylate reaction. *Rsc Adv.* **5**, 18997–19001 (2015).

ACKNOWLEDGEMENTS

This work was partially supported by the National Natural Science Foundation of China (62075064), the Key R&D Program of Guangzhou (202007020003), the Guangdong Basic and Applied Basic Research Foundation (2021B1515020095, 2021A1515110919), and the Fundamental Research Funds for the Central Universities (2022ZYGXZR003).

AUTHOR CONTRIBUTIONS

J.L.G. conceived the idea. Y.C.H., H.J.L. and J.J.L. performed the experiments. Y.C.H., N.L., L.H.L. and P.X.X. analyzed the data. Y.C.H. and J.L.G. wrote the manuscript. All authors commented on the manuscript. J.L.G. and Z.M.Y. supervised the project.

COMPETING INTERESTS

The authors declare no competing interests.

ADDITIONAL INFORMATION

Supplementary information The online version contains supplementary material available at https://doi.org/10.1038/s41528-023-00281-0.

Correspondence and requests for materials should be addressed to Jiulin Gan or Zhongmin Yang.

Reprints and permission information is available at http://www.nature.com/reprints

Publisher's note Springer Nature remains neutral with regard to jurisdictional claims in published maps and institutional affiliations.